Optik - International Journal for Light and Electron Optics 264 (2022) 169428

Contents lists available at ScienceDirect

Optik

journal homepage: www.elsevier.com/locate/ijleo

Femtosecond pulsed laser ablation for paint removal at oblique illumination: Effect of the incidence angle

Alicia Moreno, Ana J. López *, Javier Lamas, Alberto Ramil

CITENI, Ferrol Industrial Campus, University of A Coruña, 15471 Ferrol, Spain

ARTICLE INFO

Keywords:
Femtosecond laser
Oblique incidence
Ablation
Paint removal
Tilted surfaces

ABSTRACT

This research studies how the angle of incidence affects the ablation process when a pulsed femtosecond laser with a wavelength of 1040 nm and a high repetition rate is applied to spray paints used for graffiti. Flat test samples were painted using four different spray paints (red, blue, black and silver). All paints had an organic base but different physicochemical properties. For each paint, the ablation process was characterized using confocal microscopy, determining the threshold fluence and the penetration depth of the laser radiation at normal incidence. For different sample tilt angles in the range of 0°–60°, the effect of oblique incidence was analysed in terms of its effect on the ablation rate and the geometric properties (depth and width) of the ablation grooves on each paint. The results show a clear decrease in the ablation rate as the angle of incidence moves away from normal incidence. Moreover, it can also be observed that for a given angle, groove depth is the property most affected by beam tilt. These results represent a necessary step in addressing both cleaning and other laser ablation processes on non-flat surfaces in a controlled and reproducible manner.

1. Introduction

Laser cleaning is a technique that allows the controlled removal of surface contaminants from the bulk of a material [1]. Since the 1980 s, it has been applied in different industrial fields, such as aerospace, automotive, tool/die and nuclear industries[2], as well as in Heritage Conservation[3–5] or biomedicine [6], among others. In comparison with conventional surface cleaning methods such as mechanical cleaning, chemical cleaning and ultrasonic cleaning, laser cleaning has the advantage of being a non-contact selective and environmentally friendly technique [7]. Additionally, combined with industrial robots, laser cleaning technology can accurately clean pollutants on large and complex structures, greatly improving quality and efficiency ([8] and references therein).

Ultrashort pulse lasers (picosecond and femtosecond length pulses) have been considered highly effective, non-thermal sources for cleaning and decoating purposes[9] and, although ultrafast lasers are currently used widely for both fundamental research and practical applications [10,11], their use for cleaning is rarely reported. In industrial settings, high power picosecond pulsed lasers have been used to remove coatings from tungsten carbide tool inserts [12]; the feasibility of the femtosecond laser as a tool for surface cleaning of aerospace components and for surface cleaning of commercial Ti-6Al-4V alloys [13,14] has also been investigated. In the field of Cultural Heritage, there are more examples of ultrashort pulsed lasers for the removal of different crusts or coatings in a variety of materials like stones, parchment, paint, wood or metal [15–24]. On the other hand, some works have been reported on femtosecond

* Corresponding author.
E-mail addresses: alicia.moreno@udc.es (A. Moreno), ana.xesus.lopez@udc.es (A.J. López), jlamas@udc.es (J. Lamas), alberto.ramil@udc.es (A. Ramil).

https://doi.org/10.1016/j.ijleo.2022.169428
Received 9 May 2022; Accepted 1 June 2022
Available online 6 June 2022

laser ablation for the functionalization of paint layers to control wettability [25] and to improve paint adhesion in automotive applications [26], but research on femtosecond laser ablation for paint stripping remains significantly unexplored. Considering that the composition of paints is a mixture of different pigments, resins and other additives designed to enhance specific properties, their complex chemical nature and, consequently, the response of different types of paints to femtosecond laser irradiation can be challenging.

Moreover, almost all previous studies on laser cleaning have been carried out in cases where the ablative laser pulse hits the surface of the material at normal incidence, but in the case of non-planar surfaces or 3D objects, it is necessary to analyse the effects that the oblique incidence has on ablation [27]. In this sense, the ablation threshold fluence with incidence angle for dielectric (soda-lime glass), semiconductor (Si) and metallic (Au) targets have been investigated [28], and it has been found that threshold laser fluence increases with the angle of incidence for polyimide targets [29] and that the ablation threshold depends on both polarization and the incident angle of the laser beam [30]. A numerical model describing the femtosecond laser ablation of copper at an oblique angle of incidence, taking into account the dynamic properties of reflectivity at high temperatures and the changes of laser fluence and spot size depending on the angle, has also been proposed [31]. Recently, [32], an angle-dependent ablation process model for picosecond pulsed laser ablation of dielectric rods was introduced; this model predicts macroscopic ablation volumes and ablation efficiencies of dielectric materials as a result of the incidence angle, which leads to greater coherence with experimental results.

When it comes to laser paint stripping, combining optimized laser parameters with proper scanning configuration is of vital importance in order to ensure successful results and, thus, set the foundations for applying the technique to a broader range of scenarios. In this sense, our group's previous research has looked at the process of the nanosecond pulse laser removal of graffiti paint from ornamental granitic stones by analysing the influence of paint and rock properties on cleaning efficacy [33–35], and has provided a systematic analysis of the effects of different irradiation parameters in the goal of optimizing the cleaning process [36], comparing the results obtained from laser methods with those from other conventional cleaning techniques [37,38]. The aforementioned studies were performed on flat test samples; however, the application of robotic laser systems to 3D surface cleaning [39,40] has highlighted the need to analyse the paint removal process at oblique angles of incidence in order to ensure satisfactory results.

This paper studies how oblique incidence affects the ablation process when a pulsed femtosecond laser with a wavelength of 1040 nm and a high repetition rate is applied to spray paint (graffiti paint). Four different types of spray paint were used, all of which had been previously employed by us during prior research. They are produced by the same brand but have different physicochemical properties. For each paint, the ablation process was analysed by determining the threshold fluence and the penetration depth of the laser radiation at normal incidence. Subsequently, the effect of oblique incidence was studied by analysing both the ablation rate and geometric features (depth and width) of the ablation grooves created on each paint at different angles of incidence. To the best of our knowledge, this is the first research looking at ultrashort pulse laser paint removal at an oblique incidence. The results of our research show a clear decrease in the ablation rate as the incidence moves away from normal incidence. Moreover, they also show that the depth of ablation grooves is the property most affected by beam tilt.

2. Materials and methods

2.1. Laser system

The laser used was the Spirit system from Spectra Physics with emission wavelength 1040 nm and pulse width < 400 fs. The intensity profile at the laser output was near-Gaussian ($M^2 < 1.2$) and the beam diameter at the exit of the laser head was 1.5 mm. The laser beam presents horizontal polarization ($> 100{:}1$). Pulse rate can be selected from single shot to 1 MHz, with maximum pulse

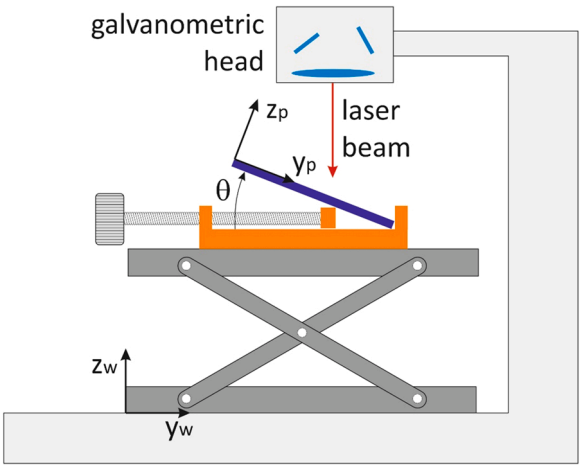

Fig. 1. Diagram of the sample stand with a micrometer screw allowing to adjust the sample tilt angle with respect to the laser beam. The reference systems for the sample (Yp, Zp) and the galvanometer scanner head (Yw, Zw) are also represented.

energy of 40 μJ at 100 kHz. The maximum mean power output is > 4 W. A two-mirror galvanometric scanner (Raylase SuperscanIII-15) was used and scanned the laser beam in X-Y directions. The beam was focused by means of a F-theta objective lens, 160 mm focal length, up to a diameter of 30 μm. At the working plane, the beam polarization is parallel to Y direction. All the processing experiments were performed in ambient air and off-line control of the ablation process was accomplished by optical microscopy (Nikon Eclipse L150) and digital image processing software.

A sample holder was included on the worktable and contained a micrometre screw that allowed us to vary the sample tilt angle with respect to the laser beam, in such a way that the value corresponding to the laser beam at an angle perpendicular to the sample piece was adopted as the initial value (angle of inclination = 0°). Fig. 1 contains a diagram of the standing device, indicating the different reference systems: Coordinates Yw and Zw refer to the worktable and Yp and Zp refer to the plane of the plate. Ablation was performed following parallel lines in the Xp direction. The necessary coordinate transformations were carried out in order to maintain a consistent distance to the beam's focal point along each line.

2.2. Evaluation of the laser effects

A Sensofar Plu 2300 confocal microscope with a XY motorized stage and using a 10x EPI objective (Field of View (1270 × 960) μm^2, resolution 768 × 576 pixels, Z-scan resolution 0.1 μm) was used to evaluate the results of the ablation process. The same device as in Fig. 1 was used to position the samples at an appropriate tilt in order to take measurements. Data processing, analysis and visualization were implemented by using Scientific Phyton. The same equipment was used to characterize the surface roughness of samples prior to laser processing; the surface roughness parameters were determined in accordance with standard UNE-EN ISO 25178–2 [41].

Confocal topographies, obtained by fitting groove profiles to a Gaussian curve, were used to obtain the geometric properties of the structures generated during ablation in terms of their depth and width [42,43].

2.3. Samples description and characterization

Four different Mtn®classic spray paints, specifically Ultramarine Blue (RAL code R-5002), Devil Red (R-3027), Graphite Black (R-9011) and Chrome Silver (hereinafter blue, red, black and silver, respectively), were selected to be studied. These paints have already been used in previous research on graffiti removal using a short-pulse (nanosecond) high-repetition-rate Nd:YVO4 laser operating at wavelength of 355 nm [33]. The aforementioned previous research carried out a physicochemical characterization of the paints, detecting different organic bases in their composition (an alkyd base in the case of the red, blue and black paints, and a polyethylene polyalkyd base in the case of the silver paint). Moreover, different extenders and opacifiers (mostly TiO_2) were identified in the red and blue paints; in the case of the silver paint, the existence of metallic aluminium particles was detected; in the black paint, no crystalline phase was detected. Furthermore, the diffuse reflectance spectrum in the interval of 200–2000 nm was also obtained and we observe that at the ultrashort pulse laser wavelength used in this research (λ = 1040 nm), the diffuse reflectance spectrum values are very high (around 90%) for the red, blue and silver paints. In fact, the silver paint maintains the aforementioned reflectance value throughout the wavelength interval analysed due to its high aluminium content, while, on the contrary, the black paint behaves like a good absorbing medium (very low reflectance) across the entire wavelength interval.

The paints were applied to flat 2 mm-thick pieces of commercial steel measuring (50 × 50) mm^2, ensuring complete coverage of the steel sheet surface with a paint layer approximately 35 μm thick. Following painting, the sheets were left to dry in a laboratory environment for one week. Subsequently, their surface texture was characterized using the parameters of areal roughness; S_a, the arithmetic mean value and S_q, the root mean square roughness. Table 1 presents the values obtained for each of the samples:

As we see, the highest roughness values are found in the silver paint, with S_a= (1.61 ± 0.21) μm and S_q= (2.11 ± 0.27) μm, which also has (as will be discussed later) the most irregular surface, reflected by a greater dispersion in the results; it is followed by the red paint with S_a= (0.71 ± 0.12) μm and S_q= (0.91 ± 0.14) μm; consecutively, the black paint with S_a= (0.32 ± 0.04) μm and S_q= (0.43 ± 0.05) μm; and, last of all, the blue paint, with values of S_a= (0.24 ± 0.05) μm and S_q= (0.34 ± 0.15) μm.

3. Results and discussion

3.1. Ablation thresholds

Estimates of the threshold fluence values F_{th} for the different paints were obtained by fitting to the Beer-Lambert law of radiation absorption via the experimental determination of the ablation depth Δz produced at a given fluence F; $\Delta z = \frac{1}{\alpha_{eff}} \ln\left(\frac{F}{F_{th}}\right)$, where α_{eff} is

Table 1
Arithmetic mean roughness (S_a) and root-mean-square roughness (S_q) for spray paintings.

Spray painting	S_a [μm]	S_q [μm]
blue	0.24 ± 0.05	0.34 ± 0.15
red	0.71 ± 0.12	0.91 ± 0.14
black	0.32 ± 0.04	0.43 ± 0.05
silver	1.61 ± 0.21	2.11 ± 0.27

the effective absorption coefficient. It is possible to determine the ablation threshold of a material by studying the ablation rate or depth per pulse; however, it is not easy to measure in single pulse ablation craters due to their small dimensions, which usually exceeds the diffraction limits of optical instruments [44], so that, small cavities of (0.5 × 0.5) mm^2 were made on the painted surface by generating parallel grooves. This scanning scheme was repeated several times until a depth enabling measurement with a confocal microscope was obtained. The tests were performed at normal laser incidence ($\theta = 0°$) with the beam defocused in order to achieve sufficiently low fluence values and to, thus, estimate the threshold value more accurately. Irradiation parameters were selected based on the aforementioned experience with short-pulse laser paint removal and in view of the goal of the research. Consequently, the values selected were the following: repetition rate $f = 5$ kHz; working distance $w_d = 1.5$ mm; scan speed $v = 150$ mm·s^{-1}; and line-to-line displacement 30 μm. The beam diameter was $D = 60$ μm and the overlap between consecutive pulses was $Op = 50\%$. The fluence F was changing by means of the variation in energy per pulse E_P.

Since results obtained using a short-pulse laser have already demonstrated that these spray paints were ablated at different rates, this research conducted a series of preliminary tests to determine the appropriate number of laser passes in order to obtain cavities with adequate dimensions in each paint. These tests were performed by maintaining $E_P = 40$ μJ at 100% power and increasing the number of laser passes. Fig. 2 presents the confocal image and topographic reconstruction of the cavities created on the red paint and silver paint, respectively. Greater roughness can be clearly seen in the silver paint (d) when compared to the red paint (b), which, as previously mentioned, results in a higher dispersion in roughness values in the case of the silver paint. Moreover, there are more irregularities visible at the bottom of the cavities (d), which also results in greater dispersion in the average cavity depth for this paint.

For each of the paints, cavity depth as a function of the number of laser passes is presented in Fig. 3. We observe that a single pass resulted in depth values ranging from 4.0 μm (red) to 11.8 μm (silver). As the number of passes increased, we clearly see different behaviour in each paint: the silver paint has the highest growth rate (slope), followed by the black, blue and red paints, respectively. Moreover, in the case of the blue and red paints, despite initially having the same slopes, the depth reached saturated at around 12 μm for the blue paint and 20 μm for the red paint, at 4 and 6 passes, respectively.

Therefore, to determine threshold fluence, the average cavity depth divided by the number of laser beam passes was adopted as the ablation depth, Δz. Moreover, fluence values were corrected by taking into account the absorbance of each paint at the laser wavelength ($\lambda = 1040$ nm), so that the fluence available for ablation $F_{available} = (1 - R) \cdot F$, where R is the reflectance value [3].

By fitting these values to the Beer-Lambert law using a nonlinear regression model, both the peak threshold fluence F_{th} and α_{eff} were obtained for each paint. Fig. 4 presents the results of curve fitting for the different paints. Extrapolation to ablation depth $\Delta z = 0$ gives the threshold fluence value F_{th}. In addition, the average threshold fluence $< F_{th} >$ delivered at each point on the surface was calculated to account for the overlap between pulses in the longitudinal and transverse directions (spot-to-spot and line-to-line). The

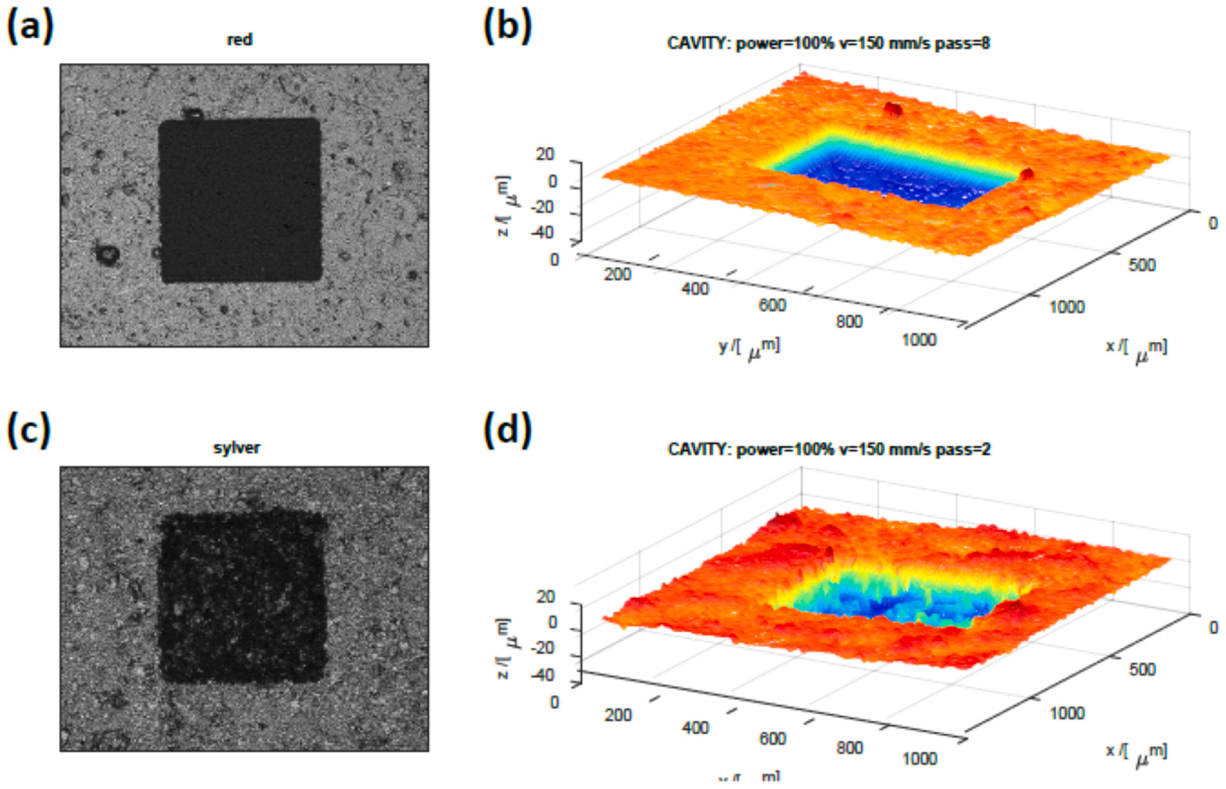

Fig. 2. Confocal image (a, c) of the red (a) and silver (c) paints and topographic reconstruction of the cavities created on the red (b) and silver (d) paints.

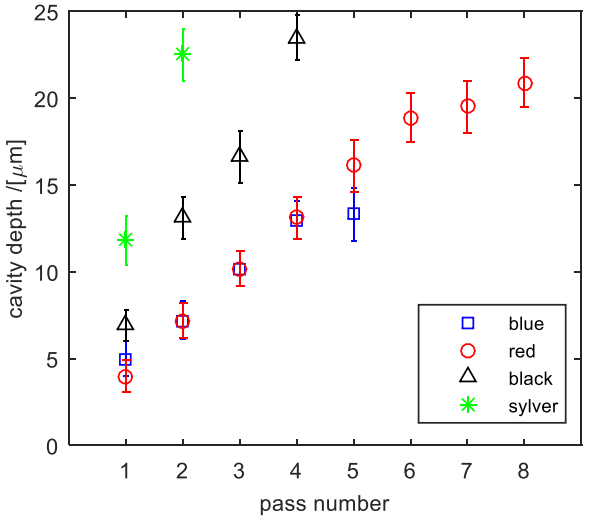

Fig. 3. Average cavity depth as a function of the number of laser passes for each paint.

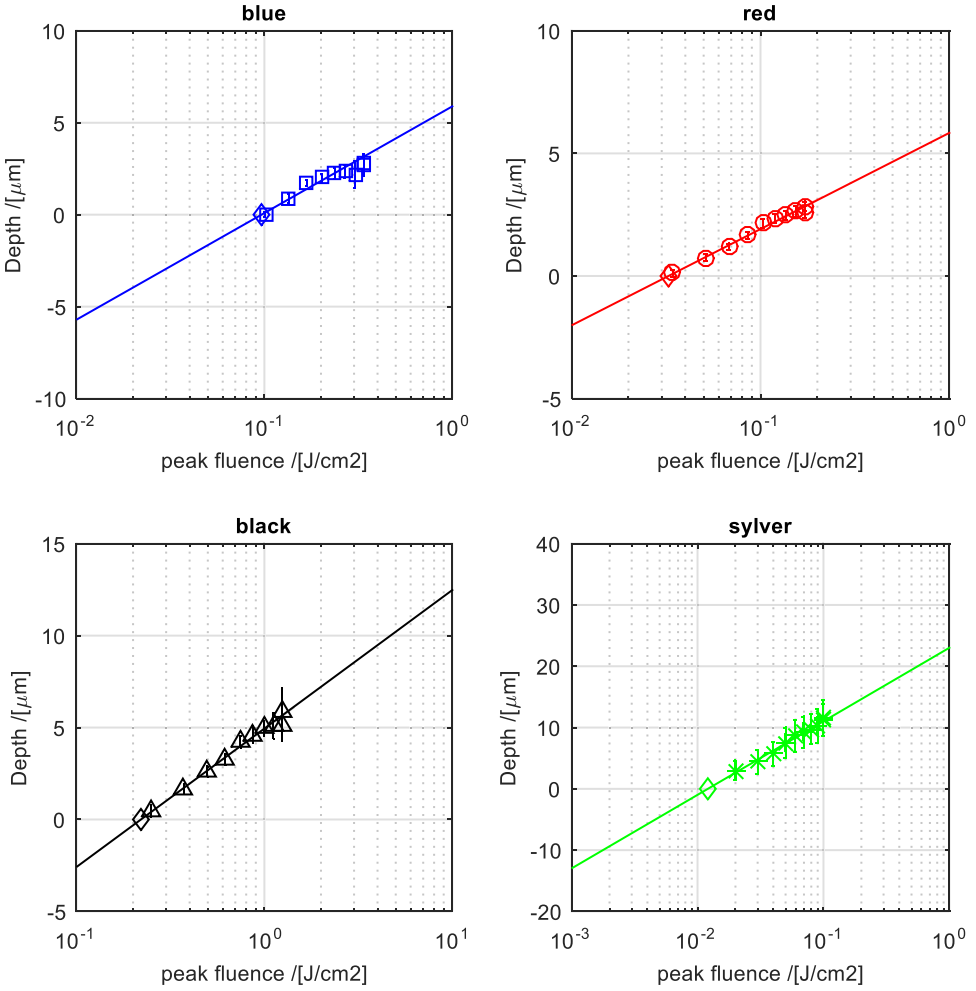

Fig. 4. Etching curves of the different paint colours by Beer's Law fit.

parameters determining this average fluence are the scan speed, v, the pulse repetition frequency f and the line-to-line spacing.

Table 2 summarizes the values obtained via curve fitting for peak threshold fluence F_{th}, average threshold fluence $< F_{th} >$ and α_{eff}, as well as the effective penetration depth values δ_{eff} ($\delta_{eff} = 1/\alpha_{eff}$) for each of the paints.

As the data in Table 2 shows, the silver paint has the lowest average threshold fluence $< F_{th} >$; therefore, less energy is required to start ablation. On the other hand, the black paint has the highest value, while the red and blue paints have similar values of $< F_{th} >$. Regarding the penetration depth δ_{eff} the silver paint once again has the highest value, in this case followed by the black, blue and red paints, respectively. The penetration depth values ($\delta_{eff} = 1/\alpha_{eff}$) are between (1.71 ± 0.06) μm for the red paint and (5.21 ± 0.22) μm for the silver paint.

The silver paint's behaviour (lower threshold fluence and higher penetration depth) can be attributed to its different physico-chemical properties, which are a result of its high aluminium content and polyalkyd base, plus the fact that it has higher surface roughness S_a and S_q values compared to the other paints. We also observe that, with respect to the blue and red paints, both of which have an organic alkyd base and similar reflectance values, the red paint has a lower roughness value than the blue paint, whereas the blue paint has a higher effective penetration value than the red paint. In this sense, different studies have shown that the ablation threshold and etching rates are dependent on polymer molecular weight [45] but also on the surface roughness; since the absorption of light depends not only on the optical properties of the material, but also on its initial surface condition[46], a higher surface roughness typically results in higher absorption of laser energy through scattering phenomena from surface irregularities, such as multiple reflection, shadowing, and back and side scattering [47]. In the case of ultrashort pulsed laser, the effect of roughness in ablation threshold in metals was also analysed and showed increased absorptivity with increasing surface roughness [48].

On the other hand, it should be noted that this behaviour observed during the ablation of the silver paint compared to the other paints clearly differs from that observed in previous research using short-pulse (ns) lasers in the UV range [33], in which the ablation efficiency for the silver paint was markedly lower than that of the other three paints.

3.2. Effect of the angle of incidence

The effect of the beam incidence angle on the efficiency of paint ablation was studied via two components: 1) the ablation rate (i.e., the ablation depth per laser pulse delivered), and 2) the size and shape (aspect ratio) of the structures generated at different angles of incidence $\theta = 0°, 30°, 45° y 60°$. To do so, ablation grooves were created, varying the scanning speed and irradiating with the beam focused (working distance $w_d = 0$, corresponding to a beam diameter $D = 40$ μm) in order to remove the largest possible amount of paint. The grooves were generated in a single laser beam pass with a pulse repetition rate $f = 5$ kHz and reducing the scan speed v applied to each paint from the same maximum value ($v_{máx} = 100$ mm s^{-1}) to a minimum value that varied as a function of each paint. As a result, the values of $v_{mín}$ range from 5 mm s^{-1} (red and blue) to 7 mm s^{-1} (black) and 10 mm s^{-1} (silver). Under these conditions, the ratio f/v (i.e. the number of pulses per unit of length) varied, with a minimum value (expressed in pulses/μm) of 0.05, 0.35 and 0.25 for the red/blue, black and silver paints, respectively. For example, Fig. 5(a) shows the profiles of the grooves created in the red paint at oblique incidence $\theta = 30°$, at scan speeds ranging from 8.3 mm·s^{-1} to 5.0 mm·s^{-1}. The average profile of each groove was fitted to a Gaussian curve, as shown in Fig. 5(b). Fitting allowed to obtain the depth and width values at oblique incidence for each of the paints.

The groove depth as a function of the number of laser pulses at normal incidence $\theta = 0°$ was analyzed first. The results are presented in Fig. 6, which shows that the depth increases linearly as a function of the number of pulses, with the silver paint having a significantly steeper slope (ablation rate) than the other paints. Specifically, the ablation rate values (expressed in μm/pulse) are: 1.4 (red), 1.6 (blue), 2.4 (black) and 3.8 (silver). These results are in line with those obtained when determining the effective penetration depth, presented in Table 2.

Fig. 7 below presents, for each paint, the groove depth as a function of the number of laser pulses at oblique incidence $\theta = 30°$, $45° y 60°$. The results for normal incidence, $\theta = 0°$, have also been included in the figure for reference purposes. We observe that, for each paint, the ablation rate decreases as the angle of incidence moves away from normal incidence. Therefore, at oblique incidence, for the same number of laser pulses delivered, n_p, the groove depth decreases; in other words, to obtain the same groove depth, it is necessary to increase n_p. We also see that the ablation rate at oblique incidence increases following the same order as in the case of normal incidence (as presented in Fig. 6: red/blue < black < silver).

Regarding groove width, at normal incidence, the ablation width is approximately equal to the spot size[42,49]. Therefore, for a Gaussian beam at normal incidence ($\theta = 0°$), the spot is circular and has a diameter $2w_0$. By varying the angle of incidence, the spot transforms into an ellipse [28,50], in such a way that as θ increases, the major axis of the ellipse grows following the ratio $2w_0/\cos\theta$, as demonstrated in Fig. 8.

Fig. 9(a) plots average groove width values as a function of $1/\cos\theta$. We observe that, for all paints, the groove width grows linearly

Table 2
Peak (F_{th}) and average ($< F_{th} >$) ablation threshold, effective absorption coefficient (α_{eff}) and effective penetration depth (δ_{eff}) for spray paintings.

Spray painting	F_{th} [J/cm2]	$< F_{th} >$ [J/cm2]	α_{eff} [1/μm]	δ_{eff} [μm]
blue	0.096 ± 0.004	0.164 ± 0.008	0.397 ± 0.031	2.52 ± 0.20
red	0.033 ± 0.001	0.079 ± 0.003	0.587 ± 0.020	1.71 ± 0.06
black	0.220 ± 0.007	0.780 ± 0.024	0.306 ± 0.010	3.27 ± 0.10
silver	0.012 ± 0.001	0.047 ± 0.003	0.192 ± 0.008	5.21 ± 0.22

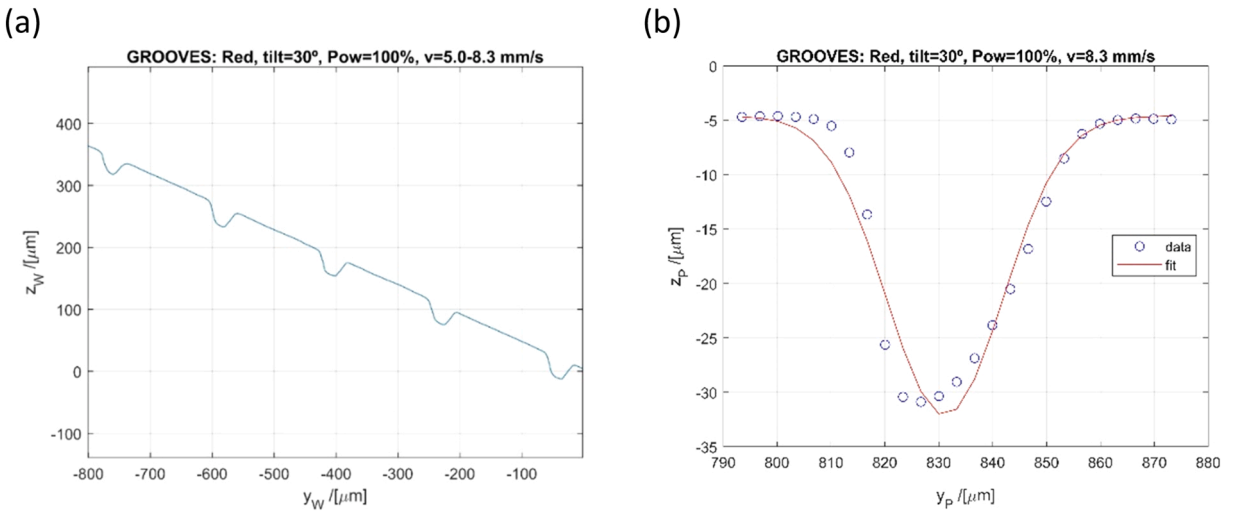

Fig. 5. (a) Profiles of the grooves created in the red paint at oblique incidence, $\theta = 30^{\circ}$, at scanning speeds ranging from 8.3 mm·s^{-1} to 5.0 mm·s^{-1}. (b) Example of fitting one of the profiles to a Gaussian curve.

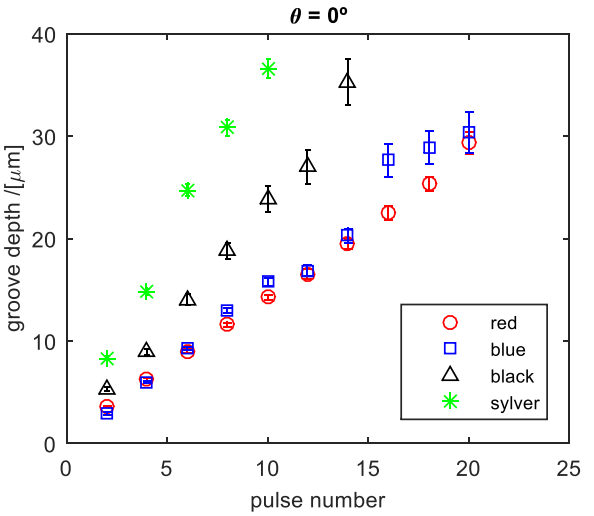

Fig. 6. Groove depth, at a 0° tilt angle, as a function of the number of laser pulses for each paint.

along with the major axis of the elliptical spot. On the other hand, an increase in spot size causes a decrease in fluence at the base of the groove following the ratio $F = (2E_P/\pi w_0^2)\cos\theta$, resulting in shallower grooves as the tilt angle increases. This is clearly observable in Fig. 9(b), which plots the ablation rate against $\cos\theta$. The ablation rate grows in a linear fashion along with $\cos\theta$; in other words, the ablation rate, and, therefore, the ablation depth, decreases as the angle of incidence moves away from normal incidence.

On the other hand, independent of the angle of incidence, the variation in groove width as a function of depth is minimal, as observable in Fig. 10, which plots width against depth for red paint for different values of θ. This behavior was observed in all paints tested. We have also included images of the grooves for each tilt angle, obtained via confocal microscopy. It is clear that for $\theta = 60^{\circ}$, wider and less well-defined grooves are obtained: this is why we observe more dispersion in width values at this tilt angle. As we can see, for a given angle of incidence, the groove width remains practically constant, independent of the depth obtained.

Therefore, these results show that, for each angle of incidence θ, groove depth is the property affected. Furthermore, the ablation rate (and, therefore, the amount of material removed) decreases along with this parameter; in other words, varying the angle of incidence with respect to normal incidence results in a decrease in the efficiency of paint ablation. Consequently, in the case of tilted or non-flat surfaces, the results obtained indicate a need to adjust the beam's angle of incidence at each point on the surface profile in order to achieve effective and uniform paint removal across the surface as a whole.

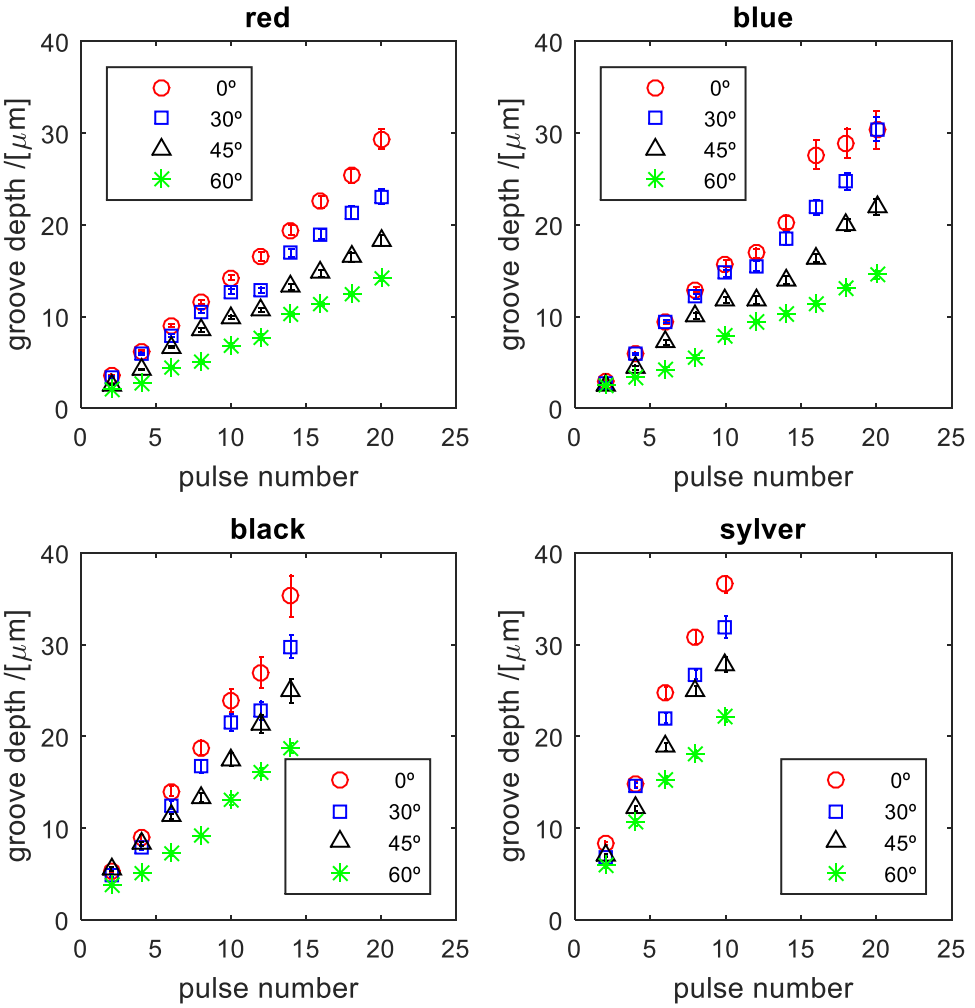

Fig. 7. Groove depth as a function of the number of laser pulses for each tilt angle.

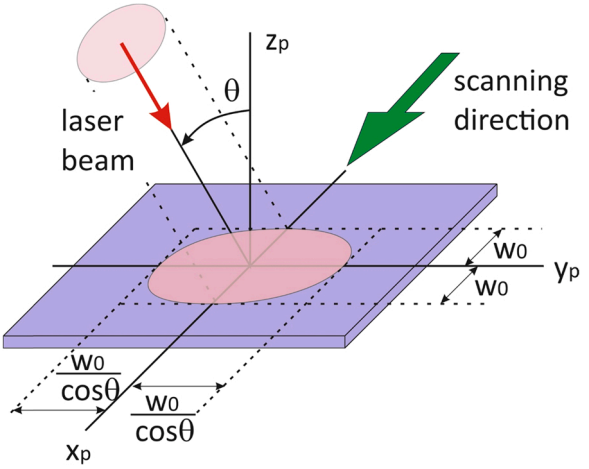

Fig. 8. Representation of ablation at oblique incidence angle θ. The circular spot of the Gaussian beam with radius w_0 at normal incidence is transformed into a ellipse with half-axis $w_0/\cos\theta$ in the direction perpendicular to the scanning direction.

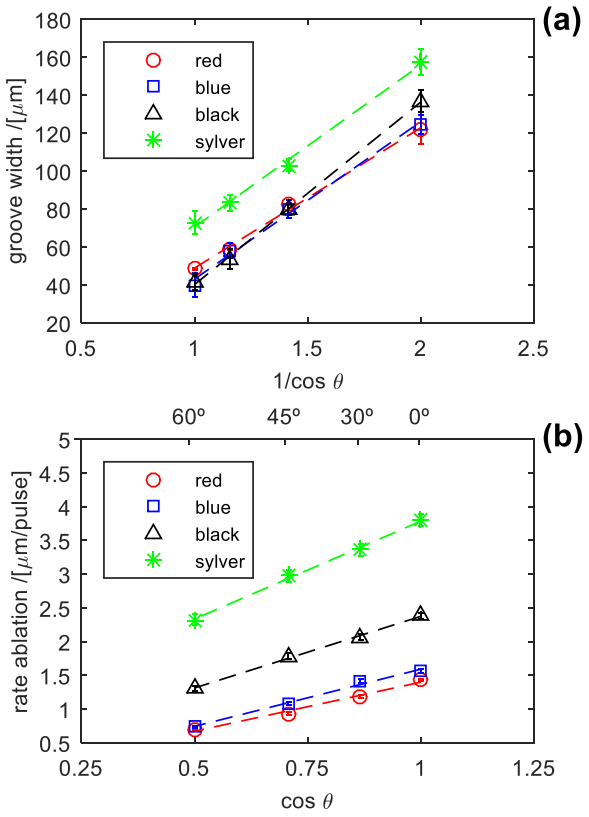

Fig. 9. Behaviour of the groove width and depth with the tilt angle θ: (a) width as a function of $1/\cos\theta$ and (b) rate ablation as a function of $\cos\theta$ for each paint.

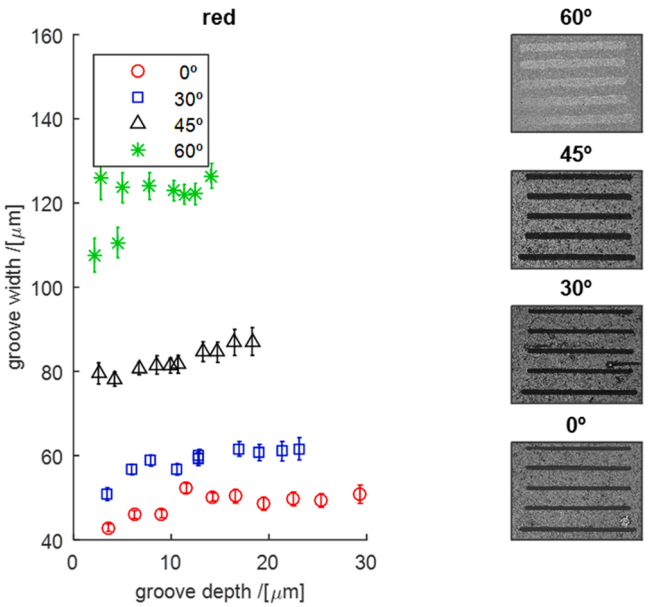

Fig. 10. Behaviour of the groove width (red paint): width as a function of depth and confocal images of grooves for each tilt angle.

4. Conclusions

This research looks at the effect of the angle of incidence of the laser beam on paint ablation using a femtosecond pulsed laser at a wavelength of 1040 nm. Both normal incidence (angle of incidence $\theta = 0$) and oblique incidence for angles $\theta = 30^{\circ}, 45^{\circ} y 60^{\circ}$ were analysed.

Four spray paint colours were considered: black, blue, red and silver. Each had different physicochemical properties and different surface roughness values, resulting in different values for threshold fluence and effective penetration depth at normal incidence, which range from (1.71 ± 0.06) μm in the case of the red paint to (5.21 ± 0.22) μm in the case of the silver paint. As a result, the ablation rate varied from 1.4 μm/pulse for the red paint to 3.8 μm/pulse for the silver paint, with the paint order in terms of ablation rate consisting of red-blue-black-silver. This outcome contrasts with that previously obtained for silver paint using a short-pulse laser in the UV regime.

At oblique incidence, the ablation rate decreases as the tilt angle increases, or, in other words, as the incidence moves away from normal incidence. In addition, the ablation rate is different for each paint, but follows the same increasing order as for normal incidence $\theta = 0^{\circ}$. Regarding the geometric properties of the grooves generated (depth and width), we observe that, as θ increases, the groove depth decreases; meanwhile, the groove width increases. On the other hand, we observe that, for a given angle of incidence, the variation in groove width as a function of depth is minimal.

To the best of our knowledge, this is the first research looking at paint removal using an ultrashort pulse laser at oblique incidence. Its results are a necessary step in addressing the topic of the laser ablation cleaning of non-flat or 3D surfaces, since they allow to quantify the effect of oblique incidence on the femtosecond laser ablation process. Moreover, it highlights the need to develop positioning and orientation systems that make it possible to adjust the angle of incidence of the laser beam at each point on the surface, in order to both optimize cleaning (maximizing the amount of material removed) and achieve uniform cleaning of 3D surfaces or surfaces with a complex geometry.

Last of all, these results can be applied to other processes based on laser ablation, such as micromachining or surface texturing, enabling advancement in the use of ultrashort pulse lasers for the processing of non-flat surfaces.

Declaration of Competing Interest

The authors declare that they have no known competing financial interests or personal relationships that could have appeared to influence the work reported in this paper.

Acknowledgements

This research was funded by the Spanish Ministry of Economy and Competitiveness under grant number BIA2017–85897-R. Funding for open access charge: Universidade da Coruña/CISUG.

References

[1] B. Luk'yanchuk, Laser Cleaning, World Scientific, 2002, https://doi.org/10.1142/4952.
[2] S. Marimuthu, H.K. Sezer, A.M. Kamara, Applications of laser cleaning process in high value manufacturing industries, Dev. Surf. Contam. Clean.: Appl. Clean. Tech. Volume 11 (2019) 251–288, https://doi.org/10.1016/B978-0-12-815577-6.00007-4.
[3] S. Siano, J. Agresti, I. Cacciari, D. Ciofini, M. Mascalchi, I. Osticioli, A.A. Mencaglia, Laser cleaning in conservation of stone, metal, and painted artifacts: state of the art and new insights on the use of the Nd:YAG lasers, Appl. Phys. A: Mater. Sci. Process. 106 (2012) 419–446, https://doi.org/10.1007/S00339-011-6690-8/FIGURES/34.
[4] A.J. López, T. Rivas, J. Lamas, A. Ramil, A. Yáñez, Optimisation of laser removal of biological crusts in granites, Appl. Phys. A 2010 100 (3. 100) (2010) 733–739, https://doi.org/10.1007/S00339-010-5652-X.
[5] P. Pouli, M. Oujja, M. Castillejo, Practical issues in laser cleaning of stone and painted artefacts: optimisation procedures and side effects, Appl. Phys. A: Mater. Sci. Process. 106 (2012) 447–464, https://doi.org/10.1007/S00339-011-6696-2/FIGURES/15.
[6] A.A. Al-Hashedi, M. Laurenti, V. Benhamou, F. Tamimi, Decontamination of titanium implants using physical methods, Clin. Oral. Implants Res. 28 (2017) 1013–1021, https://doi.org/10.1111/CLR.12914.
[7] W.M. Steen, J. Mazumder, Laser material processing: fourth edition, Laser Mater. Process.: Fourth Ed. (2010) 1–558, https://doi.org/10.1007/978-1-84996-062-5.
[8] D. Zhang, J. Xu, Z. Li, K. Li, C. Wang, D. Shan, B. Guo, Removal mechanism of blue paint on aluminum alloy substrate during surface cleaning using nanosecond pulsed laser, Opt. Laser Technol. 149 (2022), https://doi.org/10.1016/J.OPTLASTEC.2022.107882.
[9] A.V. Rode, D. Freeman, K.G.H. Baldwin, A. Wain, O. Uteza, P. Delaporte, Scanning the laser beam for ultrafast pulse laser cleaning of paint, Appl. Phys. A: Mater. Sci. Process. 93 (2008) 135–139, https://doi.org/10.1007/S00339-008-4656-2.
[10] K. Sugioka, Progress in ultrafast laser processing and future prospects, Nanophotonics 6 (2017) 393–413, https://doi.org/10.1515/NANOPH-2016-0004.
[11] G. Raciukaitis, Ultra-short pulse lasers for microfabrication: a review, IEEE J. Sel. Top. Quantum Electron. 27 (2021), https://doi.org/10.1109/JSTQE.2021.3097009.
[12] J. Ouyang, P.T. Mativenga, Z. Liu, L. Li, Energy consumption and process characteristics of picosecond laser de-coating of cutting tools, J. Clean. Prod. 290 (2021), 125815, https://doi.org/10.1016/j.jclepro.2021.125815.
[13] N. Maharjan, W. Zhou, H. Zheng, Y. Zhou, N. Wu, Surface cleaning of a titanium alloy using femtosecond laser pulses, Lasers Eng. 43 (2019) 223–235.
[14] N. Maharjan, W. Zhou, Y. Zhou, Y. Guan, Femtosecond laser cleaning for aerospace manufacturing and remanufacturing, 2017 Conference on Lasers and Electro-Optics Pacific Rim, CLEO-PR 2017. 2017-January (2017) 1–4. https://doi.org/10.1109/CLEOPR.2017.8119087.
[15] A.V. Rode, K.G.H. Baldwin, A. Wain, N.R. Madsen, D. Freeman, P. Delaporte, B. Luther-Davies, Ultrafast laser ablation for restoration of heritage objects, Appl. Surf. Sci. 254 (2008) 3137–3146, https://doi.org/10.1016/j.apsusc.2007.10.106.
[16] P. Pouli, A. Nevin, A. Andreotti, P. Colombini, S. Georgiou, C. Fotakis, Laser assisted removal of synthetic painting-conservation materials using UV radiation of ns and fs pulse duration: morphological studies on model samples, Appl. Surf. Sci. 255 (2009) 4955–4960, https://doi.org/10.1016/j.apsusc.2008.12.049.

[17] A. Elnaggar, P. Fitzsimons, A. Lama, Y. Fletcher, P. Antunes, K.G. Watkins, Feasibility of ultrafast picosecond laser cleaning of soiling on historical leather buckles, Herit. Sci. 4 (2016), https://doi.org/10.1186/S40494-016-0104-3.

[18] T. Rivas, A.J. Lopez, A. Ramil, S. Pozo, M.P. Fiorucci, M.E.L. de Silanes, A. García, J.R.V. de Aldana, C. Romero, P. Moreno, Comparative study of ornamental granite cleaning using femtosecond and nanosecond pulsed lasers, Appl. Surf. Sci. 278 (2013) 226–233, https://doi.org/10.1016/j.apsusc.2012.12.038.

[19] C.Y. Boynukara, M. Uguryol, G. Mavili, S. Akturk, An investigation of the cleaning performances of femtosecond and nanosecond laser pulses for artificially soiled papers with sizing, Appl. Phys. A: Mater. Sci. Process. 127 (2021), https://doi.org/10.1007/S00339-021-04437-5.

[20] T. Burmester, M. Meier, H. Haferkamp, S. Barcikowski, J. Bunte, A. Ostendorf, Femtosecond Laser Cleaning of Metallic Cultural Heritage and Antique Artworks, (2005) 61–69. https://doi.org/10.1007/3–540-27176–7_8.

[21] S. Gaspard, M. Oujja, M. Castillejo, P. Moreno, C. Méndez, A. García, C. Domingo, Femtosecond laser cleaning of paintings: Modifications of tempera paints by Femtosecond laser irradiation, in: Lasers in the Conservation of Artworks - Proceedings of the International Conference LACONA 7, 2008: pp. 41–47.

[22] M. Walczak, M. Oujja, L. Crespo-Arcá, A. García, C. Méndez, P. Moreno, C. Domingo, M. Castillejo, Evaluation of femtosecond laser pulse irradiation of ancient parchment, Appl. Surf. Sci. 255 (2008) 3179–3183, https://doi.org/10.1016/j.apsusc.2008.09.011.

[23] B.A. Schmidt, S. Pentzien, A. Conradi, J. Krüger, Femtosecond and nanosecond laser decontaminations of biocidal-loaded wooden artworks, Appl. Phys. A: Mater. Sci. Process. 123 (2017), https://doi.org/10.1007/S00339-017-1316-4.

[24] J. Brand, A.V. Rode, S. Madden, A. Wain, P.L. King, L. Rapp, Ultrashort pulsed laser ablation of granite for stone conservation, Opt. Laser Technol. 151 (2022), 108057, https://doi.org/10.1016/J.OPTLASTEC.2022.108057.

[25] M. Martinez-Calderon, T.A. Haase, N.I. Novikova, F.S. Wells, J. Low, G.R. Willmott, N.G.R. Broderick, C. Aguergaray, Turning industrial paints superhydrophobic via femtosecond laser surface hierarchical structuring, Prog. Org. Coat. 163 (2022), 106625, https://doi.org/10.1016/J.PORGCOAT.2021.106625.

[26] A. Guarnaccio, C. Belviso, P. Montano, F. Toschi, S. Orlando, G. Ciaccio, S. Ferreri, D. Trevisan, D. Mollica, G.P. Parisi, P. Dolce, A. Bellucci, A. De Stefanis, D. M. Trucchi, V. Valentini, A. Santagata, F. Cavalcante, A. Lettino, L. Medici, P.P. Ragone, V.G. Lambertini, Femtosecond laser surface texturing of polypropylene copolymer for automotive paint applications, Surf. Coat. Technol. 406 (2021), 126727, https://doi.org/10.1016/j.surfcoat.2020.126727.

[27] B. Scheiner, M. Schmitt, The role of incidence angle in the laser ablation of a planar target, Phys. Plasmas 26 (2019), 024502, https://doi.org/10.1063/1.5085122.

[28] X.-L. Liu, W. Cheng, M. Petrarca, P. Polynkin, Universal threshold for femtosecond laser ablation with oblique illumination, Appl. Phys. Lett. 109 (2016), 161604, https://doi.org/10.1063/1.4965850.

[29] B.S. Haq, H.U. Khan, K. Alam, M. Mateenullah, S. Attaullah, I. Zari, Femtosecond pulsed laser ablation of polyimide at oblique angles for medical applications, Appl. Opt. 54 (2015) 7413, https://doi.org/10.1364/AO.54.007413.

[30] Y. Miyasaka, M. Hashida, T. Nishii, S. Inoue, S. Sakabe, Derivation of effective penetration depth of femtosecond laser pulses in metal from ablation rate dependence on laser fluence, incidence angle, and polarization, Appl. Phys. Lett. 106 (2015), 013101, https://doi.org/10.1063/1.4905353.

[31] L.L. Dasallas, W.O. Garcia, Numerical simulation of femtosecond pulsed laser ablation of copper for oblique angle of incidence through two-temperature model, Mater. Res. Express 5 (2018), 016518, https://doi.org/10.1088/2053-1591/aaa4e8.

[32] P. Boerner, M. Hajri, T. Wahl, J. Weixler, K. Wegener, Picosecond pulsed laser ablation of dielectric rods: Angle-dependent ablation process model for laser micromachining, J. Appl. Phys. 125 (2019), 234902, https://doi.org/10.1063/1.5092812.

[33] T. Rivas, S. Pozo, M.P. Fiorucci, A.J. López, A. Ramil, Nd:YVO4 laser removal of graffiti from granite. Influence of paint and rock properties on cleaning efficacy, Appl. Surf. Sci. 263 (2012) 563–572, https://doi.org/10.1016/j.apsusc.2012.09.110.

[34] A. Ramil, J.S. Pozo-Antonio, M.P. Fiorucci, A.J. López, T. Rivas, Detection of the optimal laser fluence ranges to clean graffiti on silicates, Constr. Build. Mater. 148 (2017) 122–130, https://doi.org/10.1016/J.CONBUILDMAT.2017.05.035.

[35] J.S. Pozo-Antonio, A. Ramil, M.P. Fiorucci, A.J. L?pez, T. Rivas, The use of hyperspectral imaging technique to detect the most suitable graffiti-cleaning procedure, Color Res. Appl. 41 (2016) 308–312, https://doi.org/10.1002/col.22032.

[36] M.P. Fiorucci, A.J. López, A. Ramil, S. Pozo, T. Rivas, Optimization of graffiti removal on natural stone by means of high repetition rate UV laser, Appl. Surf. Sci. 278 (2013) 268–272, https://doi.org/10.1016/j.apsusc.2012.10.092.

[37] J.S. Pozo-Antonio, A. Ramil, M.P. Fiorucci, A.J. López, T. Rivas, The use of hyperspectral imaging technique to detect the most suitable graffiti-cleaning procedure, Color Res. Appl. 41 (2016) 308–312, https://doi.org/10.1002/col.22032.

[38] J.S. Pozo-Antonio, T. Rivas, A.J. López, M.P. Fiorucci, A. Ramil, Effectiveness of granite cleaning procedures in cultural heritage: A review, Sci. Total Environ. 571 (2016) 1017–1028, https://doi.org/10.1016/J.SCITOTENV.2016.07.090.

[39] A. Rodríguez, A.J. López, J. Lamas, A. Moreno, A. Ramil, Development of a laser cleaning robot system for the processing of 3D surfaces, in: S. Negahdaripour, E. Stella, D. Ceglarek, C. Möller (Eds.), Multimodal Sensing and Artificial Intelligence: Technologies and Applications II, SPIE, 2021, p. 28, https://doi.org/10.1117/12.2592111.

[40] A.J. López, J. Lamas, J.S. Pozo-Antonio, T. Rivas, A. Ramil, Development of processing strategies for 3D controlled laser ablation: Application to the cleaning of stonework surfaces, Opt. Lasers Eng. 126 (2020), 105897, https://doi.org/10.1016/J.OPTLASENG.2019.105897.

[41] International Organisation of Standardization, ISO 25178–2:2012 Geometrical product specifications (GPS) — Su., ISO 25178–2:2012. Geometrical Product Specifications (GPS) — Surface Texture: Areal —Part 2: Terms, Definitions and Surface Texture Parameters. (2012). ⟨https://www.une.org/encuentra-tu-norma/busca-tu-norma/iso/?c=042785⟩ (accessed December 26, 2021).

[42] M.P. Fiorucci, A.J. López, A. Ramil, Comparative study of surface structuring of biometals by UV nanosecond Nd:YVO4 laser, Int. J. Adv. Manuf. Technol. 2014 75 (1. 75) (2014) 515–521, https://doi.org/10.1007/S00170-014-6164-1.

[43] M.P.P. Fiorucci, A.J.J. López, A. Ramil, Multi-scale characterization of topographic modifications on metallic biomaterials induced by nanosecond Nd:YVO4 laser structuring, Precis. Eng. 53 (2018) 163–168, https://doi.org/10.1016/J.PRECISIONENG.2018.03.009.

[44] M. Hajri, P. Börner, K. Wegener, An industry-relevant method to determine material-specific parameters for ultra-short pulsed laser ablation of cemented carbide, Procedia CIRP 74 (2018) 709–713, https://doi.org/10.1016/j.procir.2018.08.036.

[45] I.-A. Paun, A. Selimis, G. Bounos, G. Kecskeméti, S. Georgiou, Nanosecond and femtosecond UV laser ablation of polymers: Influence of molecular weight, Appl. Surf. Sci. 255 (2009) 9856–9860, https://doi.org/10.1016/j.apsusc.2009.04.106.

[46] D.W. Bäuerle, Laser Processing and Chemistry, Springer, 2011.

[47] M. Auinger, P. Ebbinghaus, A. Blümich, A. Erbe, Effect of surface roughness on optical heating of metals, J. Eur. Opt. Soc. - Rapid Publ. 9 (2014) 14004, https://doi.org/10.2971/JEOS.2014.14004.

[48] H. Mustafa, M. Mezera, D.T.A. Matthews, G.R.B.E. Römer, Effect of surface roughness on the ultrashort pulsed laser ablation fluence threshold of zinc and steel, Appl. Surf. Sci. 488 (2019) 10–21, https://doi.org/10.1016/J.APSUSC.2019.05.066.

[49] B. Soltani, F. Hojati, A. Daneshi, B. Azarhoushang, Simulation of the laser-material interaction of ultrashort pulse laser processing of silicon nitride workpieces and the key factors in the ablation process, (n.d.). https://doi.org/10.1007/s00170–021-07111–5/Published.

[50] I. Gutu, C. Petre, I. Mihailescu, M. Taca, E. Alexandrescu, I. Ivanov, Surface treatment with linearly polarized laser beam at oblique incidence, Opt. Laser Technol. 34 (2002) 381–388, https://doi.org/10.1016/S0030-3992(02)00032-4.